

## Quest for Impact Fast Ignition

M. Murakami 1), H. Azechi 1), H. Nagatomo 1), T. Kadono 1), K. Shigemori 1),  
Y. Hironaka 1), T. Watari 1), K. Takeda 1), T. Norimatsu 1), H. Shiraga 1), K. Mima 1),  
S. Obenschain 2), M. Karasik 2), J. Bates 2), D. Colombant 2), Y. Aglitskiy 2),  
A. Velikovich 2), A. Schmitt 2), J. Sethian 2)

1) Institute of Laser Engineering, Osaka University, Suita, Osaka 565-0871, Japan

2) Naval Research Laboratory, Washington DC 20375, USA

e-mail contact of main author: murakami-m@ile.osaka-u.ac.jp

**Abstract.** First integrated experiments for impact ignition have been performed, in which a fraction of separately accelerated deuterated polystyrene (CD) shell (the impactor) at around  $600 \text{ km s}^{-1}$  was collided with another fraction of pre-compressed CD fuel. The kinetic energies of the impactor were observed to be converted into thermal energy corresponding to temperatures of about 1.6 keV. We have observed as a result an increase of two orders of magnitude in neutron yield at the right timing of the impact collision, demonstrating the high potential of impact ignition for fusion energy production.

### 1. Introduction

Major laboratories around the world are now in a tight race to achieve thermonuclear ignition in laser fusion research. Toward this goal, we employ a new scheme called “impact ignition” [1, 2], in which a fraction of separately imploded fuel (the impactor) is accelerated to a super-high velocity on the order of  $1000 \text{ km s}^{-1}$  and collided with pre-compressed main fuel. The kinetic energy is directly converted into thermal energy corresponding to temperatures  $>50$  million degrees, and this self-heated portion plays the role of the ignitor of thermonuclear fusion. Simple physics, a high energy coupling efficiency, and low cost are the notable advantages of this scheme. Here we describe the first proof-of-principle of impact ignition: We have observed an increase of two orders of magnitude in neutron yield at the right timing of the impact collision, demonstrating the high potential of impact ignition for fusion energy production.

Thermonuclear ignition has been a long-awaited goal in laser fusion research. Researchers at the US National Ignition Facility [3] and the French Laser Mégajoule [4] are expected soon to achieve laboratory ignition. Fast ignition [5] has the potential to reach this goal with about one tenth of the laser energy required in these programs. The concept of fast ignition is to separate fuel compression from ignition, which is attained by injecting an extremely intense and short laser (so-called petawatt laser) pulse into a pre-compressed fuel. Recent studies [6, 7] have shown that a substantial fraction of the laser energy for ignition is converted into thermal energy of the compressed fuel. However, fast ignition still has many intractable physical problems to solve relevant to complex laser-matter interactions, such as the transport of the absorbed energy via hot electrons or energetic ions to the dense compressed fuel. Impact ignition is expected to eliminate this complexity while keeping the compactness advantage of fast ignition. There are also two other approaches which resort to simple hydrodynamic principle: an impulsive plasma jet flow [8] and “shock ignition” [9, 10] utilizing spherical converging shock. In this Letter we report the first experimental results on this impact ignition, demonstrating two orders-of-magnitude increase of neutron yield at a right timing of the impact collision.

## 2. Super-high Velocity Experiments

In the impact ignition concept, a fraction of a fuel (impactor) is accelerated to a super-high velocity, compressed by convergence, and collided with a pre-compressed main fuel. The impactor then becomes an igniter via shock compression and heating. The requirement of a super-high velocity of about  $1000 - 1500 \text{ km s}^{-1}$ , corresponding to 3-4 times higher than the velocity of central ignition targets, can be easily derived from energy conservation and the ignition temperature of 5-10 keV [11]. Meanwhile the impactor density in flight needs to be a few  $\text{g cm}^{-3}$  so that, after spherical convergence [12] followed by the shock compression, the igniter has a sufficiently high density (on the order of  $100 \text{ g cm}^{-3}$ ). The primary challenge is thus to simultaneously provide such high velocities and inflight densities while keeping target integrity. We have explored the feasibility of achieving the above criteria in terms of two sets of experiments as demonstrated below.

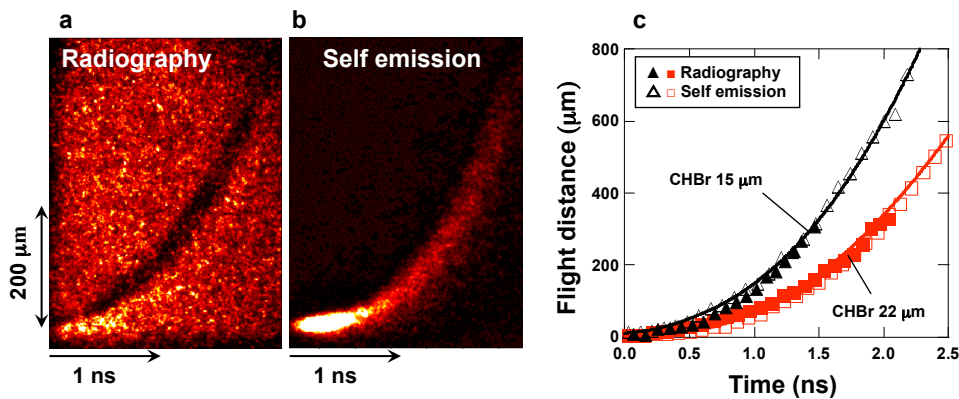
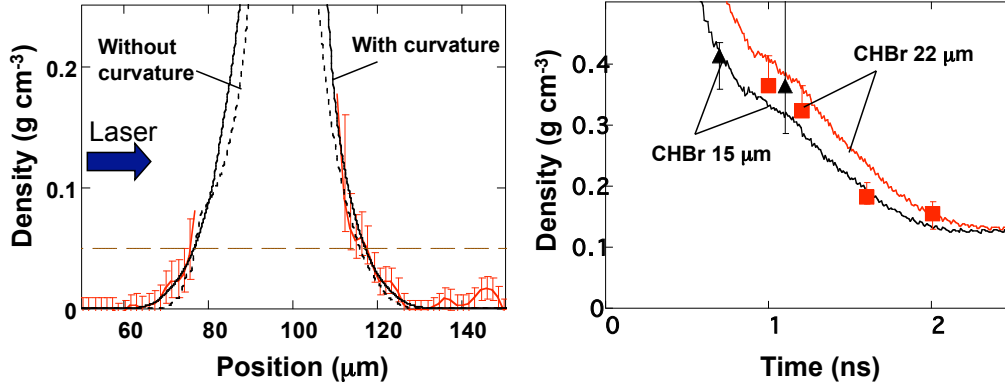


Fig.1. (a) Radiography x rays (from a separate Cu foil) were attenuated by the photo-absorption process in the target and were observed from the direction along the target surface. (b) The self-emission has peak intensity near the target surface. (c) Compiled data of the flight distance vs. time.

First we have conducted experiments on ablatively accelerating planar plastic foil targets to velocities approaching  $1000 \text{ km s}^{-1}$ . For stable and high acceleration of a laser-driven foil target, we have employed double ablation technique [13], i.e., middle-Z atoms doped in the plastic foil generate an x-ray driven ablation in addition to the electron driven ablation. Other techniques [14–16] are also plausible for stable acceleration. The targets were polystyrene doped with 0.4-atomic% bromine (CHBr) with a thickness of 15 or 22 μm, and they were irradiated with a 0.35-μm-wavelength laser at an intensity of  $400 \text{ TW cm}^{-2}$ . The trajectory of the target was observed by x ray radiography from the direction along the target surface.

Figure 1(a) shows time-resolved x ray radiography of a CHBr foil target (22-μm thickness). The time and spatial resolutions are 50 ps and 15 μm, respectively. In Fig. 1(a), the radiography x rays, which were emitted from a separate Cu foil, were attenuated by the photo-absorption process in the target and were observed from the direction along the target surface. Self-emission x rays from the target was largely attenuated by 5-μm-thick Mg and 10-μm-thick Al filters. Figure 1(b) shows the self-emission x ray from the laser-irradiated target surface, that has peak intensity near the target surface. This emission was simultaneously observed with the same geometry as that of the radiography but without the Mg and Al filters. Figure 1(c) shows the compiled data of the flight distance vs. time. The self-emission data are offset by tens of microns to compare with the radiography data. From the slopes of the

images, the terminal velocities were determined to be  $500 \text{ km s}^{-1}$  (22- $\mu\text{m}$ -thick CHBr) and  $640 \text{ km s}^{-1}$  (15- $\mu\text{m}$ -thick CHBr). The latter velocity is the highest velocity ever achieved with target integrity (shown below).



**Fig. 2.** (a) Density profiles, at 1 ns after the initial half time of the incident laser, from the radiography and a one-dimensional hydrodynamic simulation. (b) The average density vs. time obtained from the experiment and the simulation.

### 3. Measurements of In-flight Density

The target density in flight was obtained from the column mass, which was calculated as a mass-integration for a unit area along the thickness, divided by the target thickness. We estimated the residual column mass after laser ablation with the help of simulation and an experimental database of mass ablation rates. The target thickness was measured from a radiography image. Figure 2(a) shows the density profiles of the in-flight target observed with x ray radiography measured at 1 ns after the time at which the laser intensity rises to its half maximum. The errors are due to the limited photon statistics and the uncertain intensity profile before the attenuation. A potential curvature of the target, caused by a spatially non-uniform laser drive, might have blurred the image of the density profile. This curvature was computed by the hydrodynamic simulation code ILESTA-1D [17, 18] using the measured laser intensity profile. This comparison indicates the insignificance of the curvature effect. Figure 2(b) shows the average target density thus obtained. The target boundary that defines the thickness was determined as the point that gave a unit opacity corresponding to a target density of  $0.05 \text{ g cm}^{-3}$ . The agreement between the simulation and the experiment, as can be seen in Figs. 2(a) and 2(b), suggests that the target integrity was well preserved with an average density of  $0.1\text{--}0.2 \text{ g cm}^{-3}$  at the time of terminal velocity ( $t = 2\text{--}2.5 \text{ ns}$ ). The peak density is expected to be higher than the average value by a factor of 1.5–2.

### 4. Integrated Experiments

We further demonstrated the feasibility of impact ignition by colliding the impactor with a pre-compressed fuel. Figure 3(a) shows such a target for the integrated experiment of impact ignition. Both the main fuel and the impactor were irradiated by Gaussian-shaped lasers with a wavelength of  $0.53 \mu\text{m}$  and a pulse duration of  $\tau_L = 1.3 \text{ ns}$ . The main fuel was a deuterated polystyrene (CD) shell that served as a fusion fuel surrogate (500- $\mu\text{m}$  diameter, 7- $\mu\text{m}$  thickness). A gold cone with an apex angle of  $90^\circ$  was inserted into the main fuel shell. The

cone had an open apex with a diameter of 50  $\mu\text{m}$  for the impactor to transmit freely through the apex. The impactor was a CD hemispherical shell (500- $\mu\text{m}$  diameter, 10- $\mu\text{m}$

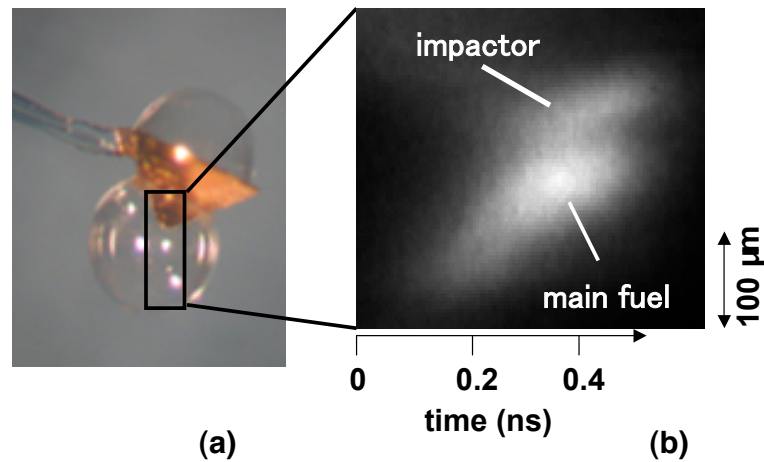


**Fig. 3.** (a) An integrated target for impact ignition. A gold cone with an open apex was inserted into a deuterated polystyrene (CD) shell. (b) Streaked x ray image showing the collision of the impactor with the pre-compressed main fuel. The time fiducial was provided by directly irradiating the gold cone with a portion of the impactor laser.

thickness) attached to the entrance of the cone. Nine out of the twelve beams of the GEKKO XII laser [19] (implosion laser) were used to irradiate the main fuel with an energy of 3 kJ. The density and temperature of the pre-compressed main fuel were inferred from experiments conducted under nearly identical laser and target conditions to be 50–100  $\text{g cm}^{-3}$  and 0.3–0.4 keV, respectively [6, 7]. As for the impactor, only a small part of the shell (0.25  $\mu\text{g}$ ) was irradiated with the remaining three beams (impactor laser) with an energy of 0.41 kJ at a laser intensity of 700  $\text{TW cm}^{-2}$ . The residual mass fraction was estimated from both the experimental database of the mass ablation rate and the simulation to be 19% of the initial mass. The terminal velocity was separately determined from the self-emission measurement to be 580  $\text{km s}^{-1}$ . These values reveal that the kinetic energy of the impactor was about 8 J corresponding to 2% of the incident laser energy. The inflight target density was probably lower than 0.1–0.2  $\text{g cm}^{-3}$ , which was observed for the CDBr targets, because the un-doped target would likely have been disintegrated by the Rayleigh-Taylor instability.

Figure 3(b) shows the collision of the impactor with the pre-compressed main fuel measured as a temporal evolution of the streaked x ray image at energies of 1-3 keV. To provide a time fiducial for the streak camera, we irradiated the edge of the gold cone with a portion of the impactor laser. Two straight emission lines on the streak image are thus provided the time fiducial. At an optimum timing between the implosion laser and the impactor laser, the impactor can be expected to collide with the main fuel in the vicinity of the initial center of the main fuel. In Fig. 3(b), one can observe two x ray emissions at a time around 1.6 ns. The first one in the image with the larger size was apparently from the main fuel, and the second emission image disappeared when we changed the timing of the impactor laser relative to the implosion laser by 300 ps or longer. These observations clearly indicate that the second emission can be attributed to the collision of the impactor with the main fuel, as it heated up and emitted x rays.

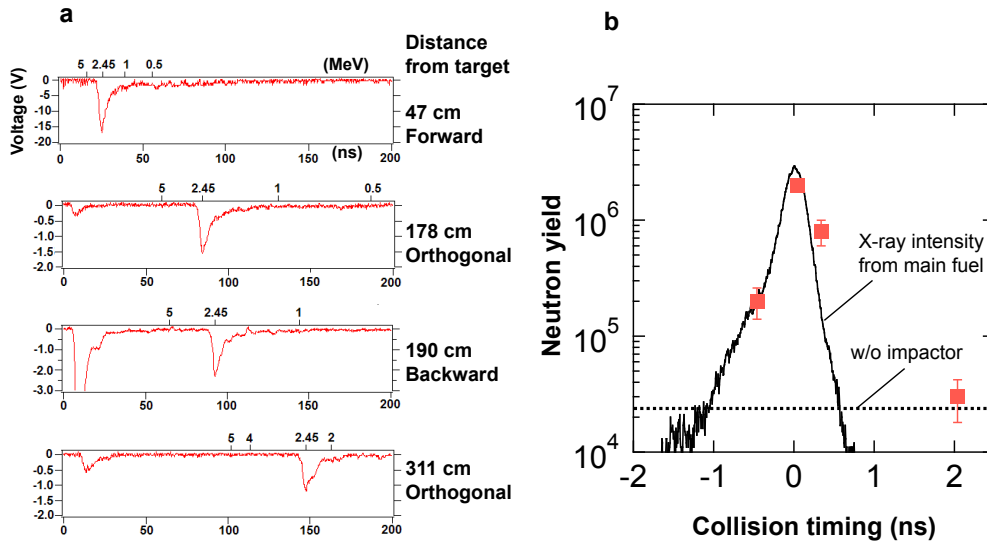


**Figure 4** (a) Time-of-flight signals of neutron emission. Neutrons were detected at different flight distances and orientations with respect to the acceleration direction of the impactor. (b) Neutron yield vs. the collision timing. The dashed line shows the neutron yield with no laser irradiation on the impactor. The solid curve represents the x ray emission pulse from the main fuel observed in Fig. 3(b).

We observed the yield and isotropy of the neutron emission with five neutron detectors, four of which were operated in current mode. These detectors consisted of fast plastic scintillators (Bicron BC422 with 1% benzophenone quencher) with either 18-cm diameter x 2.5-cm thickness or 10-cm diameter x 5-cm thickness coupled with fast photomultiplier tubes (Hamamatsu R2083). A 10-cm lead shield was placed in front of each detector. Two detectors were located in the nearly forward and backward directions with respect to the acceleration direction of the impactor, while the other two were in nearly orthogonal directions. The distances between the target and the detectors were 47, 178, 190, and 311 cm. The fifth detector was a 421-channel count mode spectrometer [20] that recorded the time-of-flight (TOF) of individual neutrons at a distance of 13.4 m from the target. From the Doppler broadening of the neutron spectrum, the ion temperature of the impactor was measured. All the detectors and the spectrometer were calibrated with respect to DD protons from a deuterium-filled glass shell imploded in the symmetrical irradiation configuration.

Figure 4(a) shows the TOF signals of four neutron emission. The distinct peaks corresponding to 2.45-MeV neutrons are confirmed. Moreover, the absolute neutron yields were consistent with each other to within about  $\pm 10\%$ , which is the statistical uncertainty of the calibration. The isotropy and no energy shift in the neutron emission thus obtained indicate that the neutrons were generated by thermonuclear fusion. As we changed the timing of the impactor laser relative to the implosion laser, the neutron yield sharply increased by two orders of magnitude at the time of the impact collision with the main fuel as shown in Fig. 4(b). The horizontal dashed line represents the neutron yield without laser irradiation on the impactor. The solid curve represents the x ray emission pulse from the main fuel observed in Fig. 3(b). The collision timing for the occurrence of peak neutron emission was obtained from the x ray emission pulse with respect to that from the main fuel. Those for the other data were obtained from the timing between the implosion laser and the impactor laser. These observations show

that the neutrons were indeed generated by the impact collision. The maximum neutron yield in this experiment was  $2 \times 10^6$  with an observed ion temperature ( $T_i$ ) of  $1.59^{+0.29}_{-0.20}$  keV.

## 5. Discussion

The fusion yield  $Y_n$  is estimated from the ion temperature  $T_i$ , the density-radius product  $\rho R$  of the impactor at the collision time, and the impactor mass  $M_{CD}$ :  $Y_n = \iint (n_D^2/2) \langle \sigma v \rangle_{DDn} dV dt \approx (\langle \sigma v \rangle_{DDn}/32c_s) M_{CD} \rho R / m_{CD}^2$ , where  $n_D$  is the deuteron density,  $\langle \sigma v \rangle_{DDn}$  the velocity-averaged DD fusion cross-section in the neutron branch,  $V$  the volume of the impactor,  $t$  the reaction time, and  $m_{CD}$  the average ion mass. The above integral is evaluated assuming that  $t$  is determined by the expansion wave passage at the sound speed  $c_s$  through the shock-compressed impactor plasma. Note that  $\langle \sigma v \rangle_{DDn}$  and  $c_s$  are both explicit functions of only the temperature. From the neutron yield, ion temperature, and residual impactor mass ( $0.25 \mu\text{g} \times 0.19$ ), we get a  $\rho R$  value and thus a corresponding density of  $1.3\text{--}9.0 \text{ g cm}^{-3}$  via mass conservation. These densities are substantially higher than the estimated inflight density measured for the planar experiments,  $0.1\text{--}0.2 \text{ g cm}^{-3}$ . This indicates that the impactor underwent conspicuously high compression due to the geometrical convergent effect.

## 6. Conclusion

Different experimental results for impact ignition have been demonstrated on the super-high velocity, the inflight density measurements, and the first integrated experiments have been performed. By extending the demonstrated velocity from  $640 \text{ km s}^{-1}$  to  $1000 \text{ km s}^{-1}$ , the inflight density from  $0.1\text{--}0.2 \text{ g cm}^{-3}$  to a few  $\text{g cm}^{-3}$ , and the energy efficiency from 2% to 10% and taking the convergence effect into account, we estimate the laser energy necessary to create a hot spark to ignite DT fusion fuel ( $T = 5 \text{ keV}$ ,  $\rho = 100 \text{ g cm}^{-3}$ , and  $\rho R = 0.4 \text{ g cm}^{-2}$ ) to be  $100\text{--}200 \text{ kJ}$  [9, 10], which is much smaller than the requirement for central spark ignition and is comparable to that for standard fast ignition [21]. Of course, we are still uncertain how the above extension can be made. Presumably this extension might require appreciably shorter wavelength lasers than that used in this study, such as KrF lasers or fourth harmonics of Nd:glass lasers. In conclusion, scaling up from the present experiments demonstrates that full-scale impact ignition could be attained within a practical allowable range.

## Reference

- [1] MURAKAMI, M., NAGATOMO, H., Nucl. Inst. & Meth. Phys. Res. **A544** (2005) 67.
- [2] MURAKAMI, M., et al., Nucl. Fusion **46** (2006) 99.
- [3] HAYNAM, C.A., et al., Appl. Opt. **46** (2007) 3276.
- [4] BIGOT, B., J. Phys. IV France **133** (2006) 3.
- [5] TABAK, M., et al., Phys. Plasmas **1** (1994) 1626.
- [6] KODAMA, R., et al., Nature **412** (2001) 798.
- [7] KODAMA, R., et al., Nature **418** (2002) 933.
- [8] VELARDE, P., et al., AIP Conf. Proc. **406** (1997) 182.
- [9] ZHOU, C., BETTI, R., Bull. Am. Phys. Soc. **50** (2005) 140.
- [10] BETTI, R., et al., Phys. Rev. Lett. **98** (2007) 155001.
- [11] ZEL'DOVICH, YA.B., RAIZER, YU.P., "Physics of shock waves and High temperature Hydrodynamic Phenomena" (Academic, New York, 1966), Chap. I.
- [12] BASKO, M.M., MEYER-TER-VEHN, J., Phys. Rev. Lett. **88** (2002) 244502.
- [13] FUJIOKA, S., et al., Phys. Rev. Lett. **92** (2004) 195001; FUJIOKA, S., et al., Phys. Plasmas **11** (2004) 2814.
- [14] LINDL, J.D., Mead, W.C., Phys. Rev. Lett. **34** (1975) 1273; MCKENTY, P.W., et al. Phys. Plasmas **8** (2001) 2315; GONCHAROV, V.N., et al., *ibid.* **10** (2003) 1906.
- [15] Bodner, S.E., et al., Phys. Plasmas **7** (2000) 2298.
- [16] K. Otani et al., Phys. Plasmas **14** (2007) 122702.
- [17] TAKABE, H., et al., Phys. Fluids **31** (1988) 2884.
- [18] SUNAHARA, A., et al., Phys. Rev. Lett. **91** (2003) 095003.
- [19] C. Yamanaka *et al.*, *IEEE J. Quantum Electron* **QE-17**, 1639 (1981).
- [20] IZUMI, N., et al., Rev. Sci. Instrum. **70** (1999) 1221.
- [21] ATZENI, S., Phys. Plasmas **6**, 3316 (1999).